Strain and Temperature Discrimination Based on a Mach-Zehnder Interferometer With Cascaded Single Mode Fibers

Shiying XIAO[1], Beilei WU[1*], Chunran SUN[2], Zixiao WANG[1], and Youchao JIANG[1]

[1]*Key Laboratory of All Optical Network and Advanced Telecommunication Network of EMC, Institute of Lightwave Technology, Beijing Jiaotong University, Beijing 100044, China*

[2]*System Integration Department, China North Industries Corp., Beijing 100053, China*

[*]Corresponding author: Beilei WU E-mail: wubeilei@bjtu.edu.cn

Abstract: An in-fiber Mach-Zehnder interferometer is proposed for the discrimination of strain and temperature. The sensor is based on two cascaded standard single mode fibers using three peanut tapers fabricated by simple splicing. The cascaded structure excites more frequency components, which induce four sets of interference dips in the transmission spectrum. One set of the spectrum dips have different sensitivities to temperature and strain from those of the other three. The sensor can discriminate strain and temperature by monitoring the wavelength shifts of two spectrum dips. Repeated experiments are taken both for strain and temperature increasing and decreasing scenarios. Experimental results show that Dip 1 has an average strain sensitivity of –0.911 pm/με and an average temperature sensitivity of 49.98 pm/℃. The strain sensitivity for Dip 2 is negligible and its average temperature sensitivity is 60.52 pm/℃ The strain and temperature resolutions are ±3.82 με and ±0.33 ℃.

Keywords: Mach-Zehnder interferometer; peanut taper; simultaneous measurement; single mode fiber; strain sensor; temperature sensor

Citation: Shiying XIAO, Beilei WU, Chunran SUN, Zixiao WANG, and Youchao JIANG, "Strain and Temperature Discrimination Based on a Mach-Zehnder Interferometer With Cascaded Single Mode Fibers," *Photonic Sensors*, 2023, 13(1): 230122.

1. Introduction

In-fiber Mach-Zehnder interferometers (MZIs) have been studied recently for various sensing applications such as the sensing of strain [1–5], temperature [6], pH [7, 8], pressure [9, 10], curvature [11, 12], humidity [13], refractive index [14–16], and magnetic field [17, 18]. An in-fiber MZI can be manufactured with multiple methods, for instance, using down-tapering structures [3], up-tapering structures [1], core-offset splicing structures [14] or simply splicing fibers with mismatched cores [4]. Among these sensors, optical fiber MZIs based on up-tapering structures, including peanut tapers and spherical tapers, have the advantages of robustness, ease-of-fabrication, and the flexibility to fabricate with fibers that either have the same or different core-cladding diameters.

Since almost all fiber optic sensors are sensitive to more than one physical parameter, dual or multiple parameter sensing attracts much research interest. For dual-parameter sensing, the focus is

Received: 30 December 2021 / Revised: 6 May 2022

DOI: 10.1007/s13320-022-0664-7
Article type: Regular

more on discriminating temperature from the target measurand. As for in-fiber MZI sensors, there are mainly three categories that are proposed for dual-parameter sensing. The most common category is the hybrid structure. This structure connects another sensor to the MZI sensor to constitute a hybrid sensor. For instance, hybrid sensors based on an MZI and a fiber Bragg grating (FBG) are demonstrated for the discrimination of temperature from the strain [1], pH [8], and magnetic field [18]. The second category is the single fiber structure which applies a single fiber, usually a special fiber, as the sensing fiber. Recently, an optical MZI sensor based on a homemade few mode fiber (FMF) is proposed for strain and temperature sensing [2] as well as for the measurement of underwater pressure and temperature [10]. Special fibers such as a side-polished fiber [16], a microfiber [9], and a ring-core fiber [12] are utilized in the MZI to discriminate temperature from the refractive index, pressure, and curvature, respectively. The third type is the cascaded structure which cascades two or more fibers for simultaneous sensing. For example, an in-fiber MZI sensor which cascades two photonic crystal fibers is proposed for measuring temperature and strain simultaneously [5]. Previously, we proposed an MZI sensor which cascaded a single mode fiber with a polarization maintaining fiber (PMF) and achieved strain and temperature discrimination [19]. Another MZI sensor cascading two hollow core fibers was proposed for discriminating gas pressure from the temperature [20].

In this paper, an in-fiber MZI sensor is proposed for the discrimination of strain and temperature. The sensor cascades two sections of the standard single mode fiber (SMF) by three peanut tapers. The cascaded structure helps to excite more frequency components, which allows more interference dips to appear in its transmission spectrum. The discrimination of strain and temperature is achieved by monitoring the wavelength shifts of two different spectrum dips. The sensor is fabricated with the standard SMF using a commercial fusion splicer. Also, the peanut taper fabricated to cascade the SMFs is a mechanical robust structure. Therefore, the proposed sensor is a robust, compact, easy-to-fabricate, and cost-effective alternative for measuring strain and temperature simultaneously.

2. Fabrication and principles

Figure 1 shows the basic structure of the proposed MZI sensor. The proposed sensor cascades two single mode fibers (SMF-28e from Corning Inc.) using three peanut tapers. The first peanut taper acts as the light splitter which helps to distribute the transmission light to the core mode and cladding modes of SMF 1. The third peanut taper acts as the light combiner which combines the light from the core mode and cladding modes of SMF 2 to the core mode of the leadout fiber. As to the second peanut taper, it acts as both light splitter and combiner which helps to redistribute the light from SMF 1 to the core mode and cladding modes of SMF 2. The peanut tapers are fabricated easily using a fusion splicer [19, 21]. The fabrication process of the peanut taper is illustrated in Fig. 2. As the figure displays, the peanut taper is fabricated with arc-discharge-A twice and arc-dischage-B once. Firstly, two SMFs are cleaved and their ends are arc discharged two times into spherical tapers with arc-discharge-A. Secondly, the same two fibers with spherical ends are arc discharged into the peanut taper with arc-discharge-B. Both arc-discharge-A and arc-dischage-B are implemented using the fusion splicer (Erisson FSU 975) with the SMF-to-SMF fusing mode with custom parameters. The second fuse time and second fuse current defined in the SMF-to-SMF fusing mode are

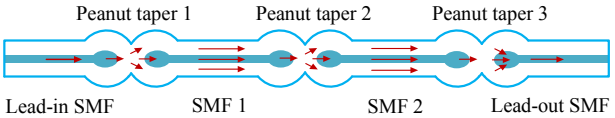

Fig. 1 Structure of the proposed sensor based on cascaded single mode fibers.

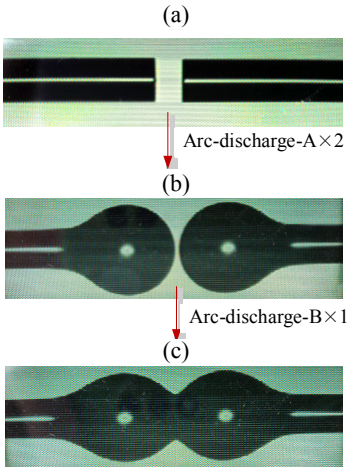

Fig. 2 Fabrication process of the peanut taper with microscopic images of (a) two cleaved SMFs, (b) SMFs with spherical end, and (c) peanut taper.

customized into 1.5 s and 25 mA for arc-discharge-A whereas 3.5 s and 15 mA for arc-discharge-B.

The proposed sensor is composed of two cascaded SMF-based MZIs. As shown in Fig. 1(a), Peanut taper 1, SMF 1, and Peanut taper 2 constitute the first MZI. Peanut taper 2, SMF 2, and Peanut taper 3 constitute the second MZI. The output intensity of the first and second MZI (I_1 and I_2) can be expressed as [15]

$$I_1 = I_{\text{core},1} + I_{\text{clad},1} + 2\sqrt{I_{\text{core},1}I_{\text{clad},1}}\cos\left(\frac{2\pi\Delta n_{\text{eff},1}L_1}{\lambda}\right) \quad (1)$$

$$I_2 = I_{\text{core},2} + I_{\text{clad},2} + 2\sqrt{I_{\text{core},2}I_{\text{clad},2}}\cos\left(\frac{2\pi\Delta n_{\text{eff},2}L_2}{\lambda}\right) \quad (2)$$

where $I_{\text{core},1}$ and $I_{\text{core},2}$ are the intensities of the core modes in SMF 1 and SMF 2, $I_{\text{clad},1}$ and $I_{\text{clad},2}$ are the intensities of the cladding modes of SMF 1 and SMF 2, $\Delta n_{\text{eff},1}$ and $\Delta n_{\text{eff},2}$ are the effective index differences between the cladding mode and the core mode, λ is the free space wavelength, and L_1 and L_2 are the lengths of SMF 1 and SMF 2. For the proposed sensor, $L_1 = L_2$. The output intensity of the cascaded sensor is [20]

$$I = I_1 I_2 = I_{A1}I_{A2} + 2I_{A1}I_{B2}\cos(\phi_1) + 2I_{A2}I_{B1}\cos\cos(\phi_2) + I_{A2}I_{B2}\left[\cos(\phi_1+\phi_2)+\cos(\phi_1-\phi_2)\right] \quad (3)$$

where $I_{A1} = I_{\text{core},1} + I_{\text{clad},1}$, $I_{A2} = I_{\text{core},2} + I_{\text{clad},2}$, $I_{B1} = \sqrt{I_{\text{core},1}I_{\text{clad},1}}$, $I_{B2} = \sqrt{I_{\text{core},2}I_{\text{clad},2}}$, $\phi_1 = 2\pi\Delta n_{\text{eff},1}L_1/\lambda$, and $\phi_2 = 2\pi\Delta n_{\text{eff},2}L_2/\lambda$. From (3), it is known that, in the transmission spectrum of the proposed sensor, there are four sets of frequency components corresponding to the phases of ϕ_1, ϕ_2, $\phi_1+\phi_2$, and $\phi_1-\phi_2$. Also, there are four sets of spectrum dips which appear when the phase match condition $\phi = (2j+1)\pi$ is satisfied (ϕ can be ϕ_1, ϕ_2, $\phi_1+\phi_2$ or $\phi_1-\phi_2$, and j is an integer). The wavelengths of the four sets of spectrum dips are

$$\lambda_1 = \frac{2\Delta n_{\text{eff},1}L_1}{2j+1} \quad (4)$$

$$\lambda_2 = \frac{2\Delta n_{\text{eff},2}L_2}{2j+1} \quad (5)$$

$$\lambda_3 = \frac{2\left(\Delta n_{\text{eff},1}L_1 + \Delta n_{\text{eff},2}L_2\right)}{2j+1} \quad (6)$$

$$\lambda_4 = \frac{2\left(\Delta n_{\text{eff},1}L_1 - \Delta n_{\text{eff},2}L_2\right)}{2j+1}. \quad (7)$$

By differentiating (4) to (7), the wavelength shifts of the four sets of spectrum dips caused by the variation of strain ($\Delta\varepsilon$) and temperature (ΔT) are determined by [21]

$$\frac{\Delta\lambda_1}{\lambda_1} = \left[1+\frac{\partial\left(\Delta n_{\text{eff},1}\right)/\partial\varepsilon}{\Delta n_{\text{eff},1}}\right]\Delta\varepsilon + \left[\frac{\partial\left(\Delta n_{\text{eff},1}\right)/\partial T}{\Delta n_{\text{eff},1}} + \frac{\partial\left(L_1\right)/\partial T}{L_1}\right]\Delta T \quad (8)$$

$$\frac{\Delta\lambda_2}{\lambda_2} = \left[1+\frac{\partial\left(\Delta n_{\text{eff},2}\right)/\partial\varepsilon}{\Delta n_{\text{eff},2}}\right]\Delta\varepsilon + \left[\frac{\partial\left(\Delta n_{\text{eff},2}\right)/\partial T}{\Delta n_{\text{eff},2}} + \frac{\partial\left(L_2\right)/\partial T}{L_2}\right]\Delta T \quad (9)$$

$$\frac{\Delta\lambda_3}{\lambda_3} \approx \left[1+\frac{1}{2}\left(\frac{\partial\left(\Delta n_{\text{eff},1}\right)/\partial\varepsilon}{\Delta n_{\text{eff},1}} + \frac{\partial\left(\Delta n_{\text{eff},2}\right)/\partial\varepsilon}{\Delta n_{\text{eff},2}}\right)\right]\Delta\varepsilon + \left[\frac{1}{2}\left(\frac{\partial\left(\Delta n_{\text{eff},1}\right)/\partial T}{\Delta n_{\text{eff},1}} + \frac{\partial\left(\Delta n_{\text{eff},2}\right)/\partial T}{\Delta n_{\text{eff},2}}\right) + \frac{1}{2}\left(\frac{\partial\left(L_1\right)/\partial T}{L_1} + \frac{\partial\left(L_2\right)/\partial T}{L_2}\right)\right]\Delta T \quad (10)$$

$$\frac{\Delta\lambda_4}{\lambda_4}\approx\left[1+\frac{\partial\left(\Delta n_{\text{eff},1}\right)/\partial\varepsilon-\partial\left(\Delta n_{\text{eff},2}\right)/\partial\varepsilon}{\Delta n_{\text{eff},1}-\Delta n_{\text{eff},2}}\right]\Delta\varepsilon+\left[\frac{\partial\left(\Delta n_{\text{eff},1}\right)/\partial T-\partial\left(\Delta n_{\text{eff},2}\right)/\partial T}{\Delta n_{\text{eff},1}-\Delta n_{\text{eff},2}}+\frac{1}{2}\left(\frac{\partial\left(L_1\right)/\partial T}{L_1}+\frac{\partial\left(L_2\right)/\partial T}{L_2}\right)\right]\Delta T. \tag{11}$$

The condition $L_1=L_2$ and the approximate condition $\Delta n_{\text{eff},1}\approx\Delta n_{\text{eff},2}$ are used for the determination of (10) and (11). From (8) to (11), it is known that the slopes of the wavelength shifts of λ_1, λ_2, and λ_3 to $\Delta\varepsilon$ and ΔT are similar while that of λ_4 is different. Therefore, it is possible to monitor one dip of λ_4 and another dip of λ_1 (or λ_2 or λ_3) in the spectrum of the proposed sensor for discriminative sensing of strain and temperature.

Figure 3(a) shows the optical spectra of the proposed MZI sensor and a single MZI with only one SMF and two peanut tapers. Their spatial frequency spectra are given and compared in Fig. 3(b). The lengths of the two SMFs in the proposed sensor are both 50 mm. The length of the SMF in the single MZI for comparison is also 50 mm. As shown in Fig. 3(b), compared with the single MZI, the proposed cascaded MZI sensor possesses more dominant frequency components in its spatial spectrum, which is consistent with the previous discussion.

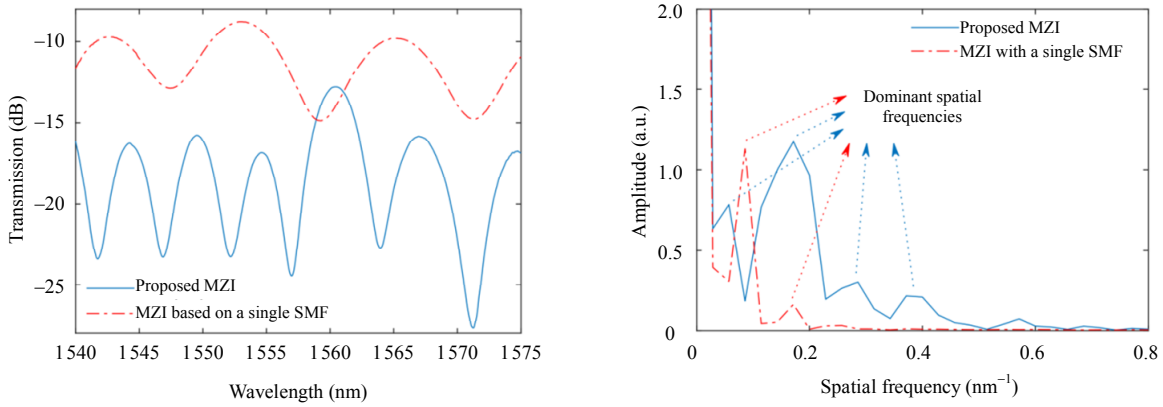

Fig. 3 Comparison of the (a) optical spectrum and (b) spatial frequency spectrum of the proposed cascaded MZI and the MZI based on a single SMF and two peanut tapers.

3. Experimental results and discussion

The experimental setups employing the proposed sensor for strain sensing and temperature sensing are illustrated in Figs. 4(a) and 4(b), respectively. An optical broadband source (BBS) and an optical spectrum analyzer (OSA) are utilized to measure the transmission spectrum of the proposed MZI sensor. For the sensing of strain, the strain applied to the sensor is implemented using a translation stage and a fixed stage. As to the sensing of temperature, the sensor is placed in a temperature chamber which is used to adjust ambient temperature.

In the strain measurement, the ambient temperature is kept at room temperature (26 ℃). The proposed sensor is straightened, with its both ends fastened on a translation stage and a fixed stage. The strain applied to the sensor is altered by adjusting the translation stage to modulate its distance from the fixed stage. The original distance (L) between the two stages is 20 cm. With this distance, no strain is applied to the sensor. When the distance increases by ΔL, the axial strain applied to the sensor is $\varepsilon=\Delta L/L$. The strain measurement experiment is repeated for 6 times. The strain increases from 0 με to 1 000 με for three times and decreases from

1 000 με to 0 με for three times at a step of 100 με.

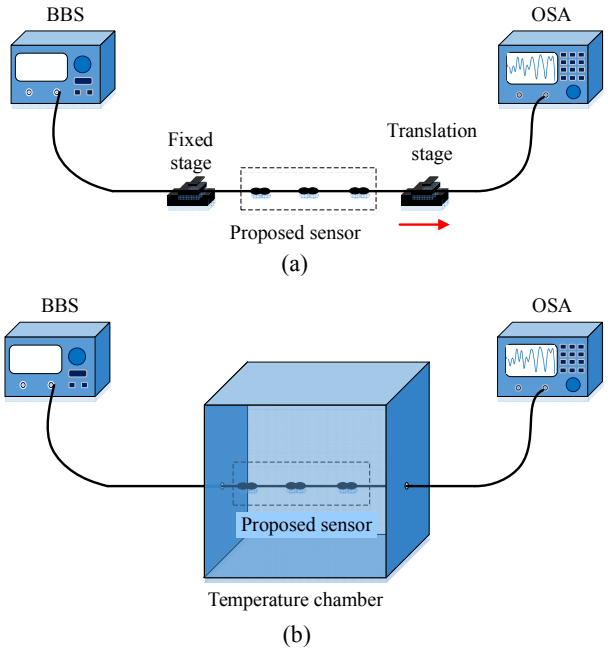

Fig. 4 Diagram of the experimental setups employing the proposed sensor for the sensing of (a) strain and (b) temperature.

Figure 5(a) illustrates the shift of the transmission spectrum of the proposed sensor in one of the strain increasing tests. As shown in Fig. 5(a), Dip 1 at 1 547 nm shows a blue shift whereas Dip 2 at 1 564 nm remains steady with an increase in strain. Figure 5(b) displays the relationships between the strain and the average wavelength shifts of the two dips for both strain increasing and decreasing tests. The error bars are obtained by calculating the standard error of the experimental data.

For the strain increasing tests, the slope of the fitted linear curve (the blue curve) of Dip 1 is –0.904 pm/με with an *R*-square of 0.990. The slope of the fitted linear curve (the red curve) of Dip 2 is -4.170×10^{-3} pm/με with a root-mean-square error (RMSE) of 0.021. For the strain decreasing tests, the slope of the fitted linear curve (the dash-dotted green curve) of Dip 1 is –0.918 pm/με with an *R*-square of 0.989. The slope of the fitted linear curve (the dash-dotted yellow curve) of Dip 2 is -1.227×10^{-2} pm/με with an RMSE of 0.017. The slopes are slightly higher in the strain decreasing tests than those in the strain increasing tests. Even so, as it is can be intuitively seen in Fig. 5(b), the difference between the experimental data caused by the increase and decrease of the strain is minimal. In addition, the slope of Dip 2 is close to zero and less than 1.34% of that of Dip 1. It means that Dip 2 can be seen as insensitive to strain variations compared with Dip 1.

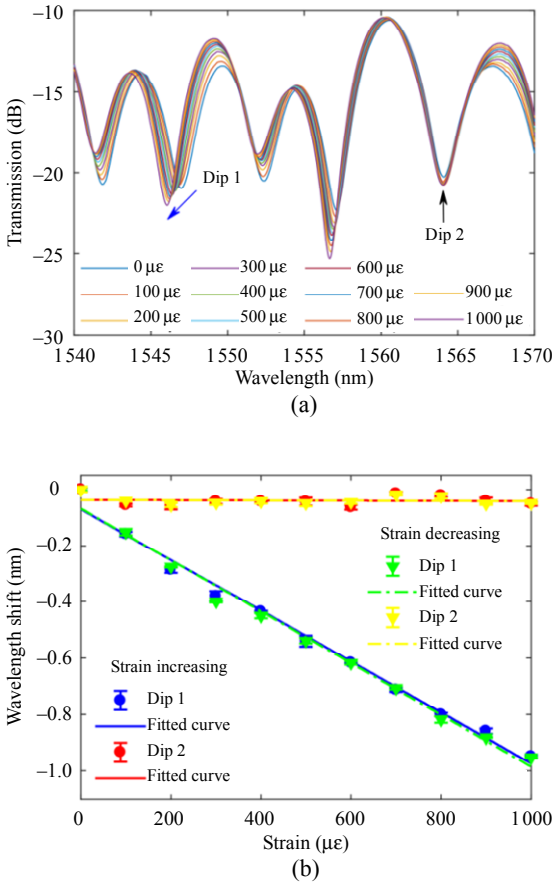

Fig. 5 Strain sensing experimental results: (a) spectrum shift of the sensor in one of the strain increasing tests, and (b) the relationship between the strain and the average wavelength shifts of Dip 1 and Dip 2 in strain increasing and decreasing experiment.

In the temperature measurement, the proposed sensor is straightened and placed in a temperature chamber with a resolution of 0.3 ℃. The temperature sensing experiment is also repeated for 6 times. The temperature increases three times and decreases three times at a step of about 5 ℃. The temperature ranges from 26 ℃ to 75 ℃. Figure 6(a) displays the spectrum shift of the proposed sensor in one of the heating tests. As the figure illustrates, both Dip 1

and Dip 2 show a red shift with an increase in the temperature. Figure 6(b) shows the relationships between the average temperature and the average wavelength shifts of the two dips in both heating and cooling tests. The error bars are also given.

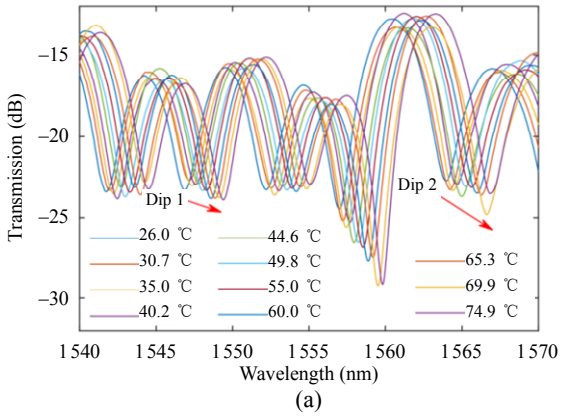

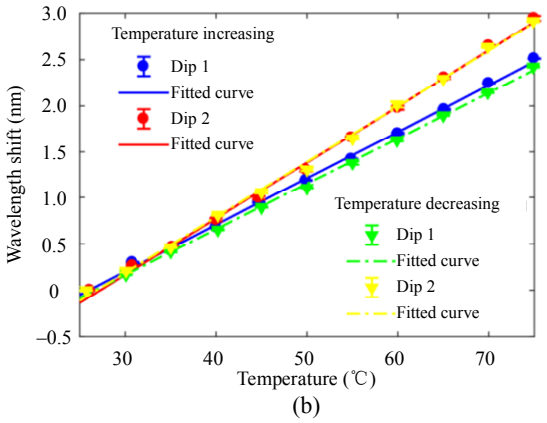

Fig. 6 Temperature sensing experimental results: (a) spectrum shift of the sensor in one of the heating tests and (b) relationship between the ambient temperature and the average wavelength shifts of Dip 1 and Dip 2 in heating and cooling experiment.

For the heating tests, the slope of the fitted linear curve (the blue curve) of Dip 1 is 50.55 pm/℃ with an *R*-square of 0.999. The slope of the fitted linear curve (the red curve) of Dip 2 is 60.84 pm/℃ with an *R*-square of 0.998. For the cooling tests, the slope of the fitted linear curve (the dash-dotted green curve) of Dip 1 is 49.42 pm/℃ with an *R*-square of 0.999. The slope of the fitted linear curve (the dash-dotted yellow curve) of Dip 2 is 60.21 pm/℃ with an *R*-square of 0.998. The slopes are slightly lower in the cooling tests than those in the heating tests. As with the case of strain sensing tests, the difference between the experimental data caused by the increase and decrease of the temperature is negligible. In addition, the difference between the two slopes of the same dip caused by the heating and cooling process is very small (<2.24%).

Since the difference between experimental data caused by the increase and decrease of strain or temperature is minimal, it is reasonable to analyze the six strain sensing tests and six temperature sensing tests altogether. Figure 7(a) shows the relationships between the strain and average wavelength shifts of Dip 1 and Dip 2 for the six strain tests. As shown in the figure, the average strain sensitivity of Dip 1 is –0.911 pm/με with an *R*-square of 0.990. The slope of the fitted curve of Dip 2 is 0.00822 pm/με, which is close to zero and less than 1 percent of that of Dip 2. Therefore, the sensitivity of Dip 2 can be regarded as zero.

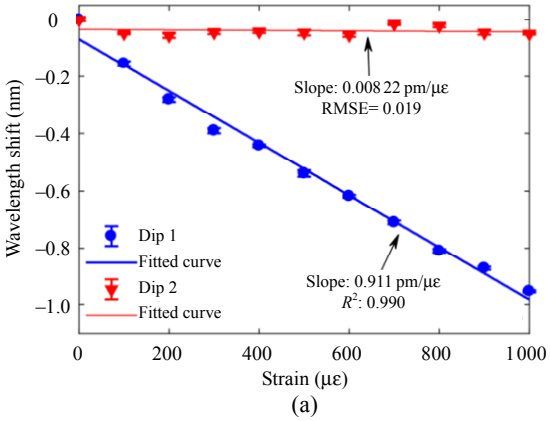

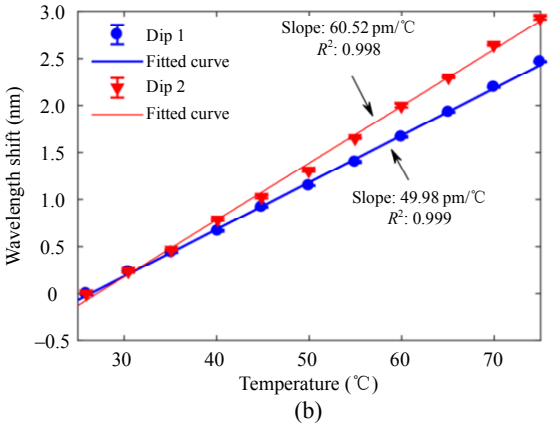

Fig. 7 Average wavelength shift versus (a) strain and (b) temperature for all experiments.

Figure 7(b) illustrates the relationships between the average temperature and the average wavelength shifts of the two dips for the six temperature tests. The average temperature sensitivity is 49.98 pm/℃ with an *R*-square of 0.999 for Dip 1 and 60.52 pm/℃ with an *R*-square of 0.998 for Dip 2.

The strain and temperature discrimination is obtained by measuring wavelength shifts of the two dips. The relationship between the wavelength shift and the strain and temperature variations is given by the following matrix [3]:

$$\begin{bmatrix} \Delta\varepsilon \\ \Delta T \end{bmatrix} = \frac{1}{C_{\varepsilon 1}C_{t2} - C_{\varepsilon 2}C_{t1}} \begin{bmatrix} C_{t1} & -C_{t2} \\ -C_{\varepsilon 2} & C_{\varepsilon 1} \end{bmatrix} \begin{bmatrix} \Delta\lambda_1 \\ \Delta\lambda_2 \end{bmatrix} \quad (12)$$

where $\Delta\lambda_1$, $C_{\varepsilon 1}$, and C_{t1} are the wavelength shift, strain sensitivity, and temperature sensitivity of Dip 1 while $\Delta\lambda_2$, $C_{\varepsilon 2}$, and C_{t2} are those of Dip 2. According to the experimental results, (12) can be rewritten for the proposed sensor as follows:

$$\begin{bmatrix} \Delta\varepsilon \\ \Delta T \end{bmatrix} = \frac{1}{-55.13} \begin{bmatrix} 60.52 & -49.98 \\ 0 & -0.911 \end{bmatrix} \begin{bmatrix} \Delta\lambda_1 \\ \Delta\lambda_2 \end{bmatrix}. \quad (13)$$

From (13), the temperature resolution (δT) and strain resolution ($\delta\varepsilon$) can be calculated by

$$\delta\varepsilon = \frac{\left|-C_{t2} + C_{t1}\right|}{\left|C_{t1}C_{\varepsilon 2} - C_{\varepsilon 1}C_{t2}\right|}\delta\lambda \quad (14)$$

$$\delta T = \frac{\left|C_{\varepsilon 2} - C_{\varepsilon 1}\right|}{\left|C_{t1}C_{\varepsilon 2} - C_{\varepsilon 1}C_{t2}\right|}\delta\lambda \quad (15)$$

where $\delta\lambda$ is the wavelength resolution. Since $\delta\lambda$ of the OSA employed in the strain and temperature tests is 20 pm, $\delta\varepsilon$ and δT are ±3.82 με and ±0.33 ℃, respectively.

The sensing properties of the proposed sensor is given and compared with several other MZI-based sensors in Table 1. As it displays in the table, for the proposed sensor, its strain and temperature sensitivities and resolutions are comparable to those of the other Mach-Zehnder interferometric sensors as a whole. It is worth mentioning that the MZI sensor based on a few mode fiber [2] and the MZI sensor based on a twisted SMF structure [22] show both high sensitivities and high resolutions. For the FMF-based sensor, its temperature resolution and strain resolution are one order higher than those of the proposed sensor. As to the sensor based on the twisted SMF structure, its strain sensitivity and strain resolution are one order higher than those of the proposed sensor. However, the fabrication of the homemade FMF and the twisted SMF is rather complicated and not readily accessible. Compared with the two sensors, the proposed SMF-based MZI sensor possesses advantages of easy fabrication and low cost because its fabrication only involves the standard single mode fiber and commercial fusion splicer. Also, the peanut taper structure used by the proposed sensor is more robust than direct splicing structure and core-offset splicing structure used by other sensors [19].

Table 1 Sensing properties of several MZI sensors for strain and temperature discrimination.

Sensing method	Sensing properties			
	Strain sensitivity (pm/με)	Temperature sensitivity (pm/℃)	Strain resolution (με)	Temperature resolution (με)
FBG and MZI based on SMF [3]	1.07 and 0.891	55.35 and 10.85	±3.104	±0.149
FPI and MZI based on micro-cavity [4]	–0.98 and 4.24	72.5 and 0.26	±4.73	±0.34
MZI based on SCF [1]	0.627 and 0	11.49 and 93.11	±1.2	±0.8
MZI based on FMF [2]	–13 and 9	–212 and 262	±4.7	±0.2
MZI based on twisted SMF [22]	34.9 and –36.19	49.23 and 62.99	±0.564	±0.357
MZI based on SMF and PMF [19]	–1.441 and -0.639	57.41 and 78.29	±5.48	±0.21
The proposed MZI based on SMF	–0.911 and 0	49.98 and 60.52	±3.82	±0.33

FPI: Fabry-Perot interferometer; SCF: seven-core fiber

4. Conclusions

An MZI sensor based on two cascaded SMFs is proposed and studied for the discriminative sensing of temperature and strain. The discriminative sensing is obtained by measuring wavelength shifts of two dips in the transmission spectrum of the

sensor. Both strain and temperature sensing experiments are repeated for 6 times. According to the experiments, the average strain sensitivity and average temperature sensitivity of Dip 1 are –0.911 pm/με and 49.98 pm/℃, respectively. The strain sensitivity of Dip 2 is negligible whereas its average temperature sensitivity is 60.52 pm/℃. In the meanwhile, the strain resolution is calculated to be ±3.82 με and the temperature resolution is ±0.33 ℃. In addition, the proposed sensor is compact, cost-effective, mechanical robust, and easy to fabrication. It is a potential alternative for measuring strain and temperature simultaneously.

Acknowledgment

This work is supported by the National Natural Science Foundation of China (Grant Nos. 62005011, 61801017, and. 62005013), the Beijing Municipal Natural Science Foundation (Grant No. 4212009), and the Fundamental Research Funds for the Central Universities (Grant No. 2020RC015).

References

[1] Y. Liu, X. Song, B. Li, J. Dong, L. Huang, D. Yu, *et al.*, "Simultaneous measurement of temperature and strain based on SCF-based MZI cascaded with FBG," *Applied Optics*, 2020, 59(30): 9476–9481.

[2] C. Lu, J. Su, X. Dong, T. Sun, and K. T. V. Grattan, "Simultaneous measurement of strain and temperature with a few-mode fiber-based sensor," *Journal of Lightwave Technology*, 2018, 36(13): 2796–2802.

[3] L. LV, S. Wang, L. Jiang, F. Zhang, Z. Cao, P. Wang, *et al.*, "Simultaneous measurement of strain and temperature by two peanut tapers with embedded fiber Bragg grating," *Applied Optics*, 2015, 54(36): 10678–10683.

[4] B. Huang, S. Xiong, Z. Chen, S. Zhu, H. Zhang, X. Huang, *et al.*, "In-fiber Mach-Zehnder interferometer exploiting a micro-cavity for strain and temperature simultaneous measurement," *IEEE Sensors Journal*, 2019, 19(14): 5632–5638.

[5] K. Naeem, Y. Chung, and B. H. Kim, "Cascaded two-core PCFs-based in-line fiber interferometer for simultaneous measurement of strain and temperature," *IEEE Sensors Journal*, 2019, 19(9): 3322–3327.

[6] L. Hou, J. Yang, X. Zhang, J. Kang, and L. Ran, "Bias-taper-based hybrid modal interferometer for simultaneous triple-parameter measurement with joint wavelength and intensity demodulation," *IEEE Sensors Journal*, 2019, 19(21): 9775–9781.

[7] R. Yan, G. Sang, B. Yin, S. Wu, M. Wang, B. Hou, *et al.*, "Temperature self-calibrated pH sensor based on GO/PVA-coated MZI cascading FBG," *Optics Express*, 2021, 29(9): 13530–13541.

[8] M. Lei, Y. N. Zhang, B. Han, Q. Zhao, A. Zhang, and D. Fu, "In-line Mach-Zehnder interferometer and FBG with smart hydrogel for simultaneous pH and temperature detection," *IEEE Sensors Journal*, 2018, 18(18): 7499–7504.

[9] Y. F. Hou, J. Wang, X. Wang, Y. P. Liao, L. Yang, E. L. Cai, *et al.*, "Simultaneous measurement of pressure and temperature in seawater with PDMS sealed microfiber Mach-Zehnder interferometer," *Journal of Lightwave Technology*, 2020, 38(22): 6412–6421.

[10] X. Lei, X. Dong, C. Lu, T. Sun, and K. T. V. Grattan, "Underwater pressure and temperature sensor based on a special dual-mode optical fiber," *IEEE Access*, 2020, 8: 146463–146471.

[11] B. Jiang, Z. Bai, C. Wang, Y. Zhao, J. Zhao, L. Zhang, *et al.*, "In-line Mach-Zehnder interferometer with D-shaped fiber grating for temperature-discriminated directional curvature measurement," *Journal of Lightwave Technology*, 2018, 36(3): 742–747.

[12] W. Yuan, Q. Zhao, L. Li, Y. Wang, and C. Yu, "Simultaneous measurement of temperature and curvature using ring-core fiber-based Mach-Zehnder interferometer," *Optics Express*, 2021, 29(12): 17915–17925.

[13] Y. Zhong, Z. Tong, W. Zhang, J. Qin, and W. Gao, "Humidity and temperature sensor based on a Mach-Zehnder interferometer with a pokal taper and peanut taper," *Applied Optics*, 2019, 58(29): 7981–7986.

[14] R. Qi, L. Xia, N. Wu, Z. Yang, and T. Ruan, "High resolution measurement of refractive index with resistance to temperature crosstalk through an all fiber MZI-PMF structure," *Sensors and Actuators A: Physical*, 2020, 302: 111790.

[15] F. Yu, P. Xue, X. Zhao, and J. Zheng, "Investigation of an in-line fiber Mach-Zehnder interferometer based on peanut-shape structure for refractive index

sensing," *Optics Communications*, 2019, 435: 173–177.

[16] P. Zhang, B. Liu, J. Liu, C. F. Xie, S. P. Wan, X. D. He, *et al.*, "Investigation of a side-polished fiber MZI and its sensing performance," *IEEE Sensors Journal*, 2020, 20(11): 5909–5914.

[17] H. Li, "In-line MZI magnetic sensor based on seven-core fiber and fiber peanut symmetrical structure," *Optical Engineering*, 2018, 57(11): 117112.

[18] R. Zhang, S. Pu, Y. Li, Y. Zhao, Z. Jia, J. Yao, *et al.*, "Mach-Zehnder interferometer cascaded with FBG for simultaneous measurement of magnetic field and temperature," *IEEE Sensors Journal*, 2019, 19(11): 4079–4083.

[19] S. Xiao, B. Wu, Z. Wang, and Y. Jiang, "A peanut taper based Mach-Zehnder interferometric sensor for strain and temperature discrimination," *Optical Fiber Technology*, 2022, 70: 102871.

[20] M. Xie, H. Gong, J. Zhang, C. L. Zhao, and X. Dong, "Vernier effect of two cascaded in-fiber Mach-Zehnder interferometers based on a spherical-shaped structure," *Applied Optics*, 2019, 58(23): 6204–6210.

[21] D. Wu, T. Zhu, K. S. Chiang, and M. Deng, "All single-mode fiber Mach-Zehnder interferometer based on two peanut-shape structures," *Journal of Lightwave Technology*, 2012, 30(5): 805–810.

[22] X. Jiang, P. Lu, Y. Sun, H. Liao, D. Liu, J. Zhang, *et al.*, "Simultaneous measurement of axial strain and temperature based on twisted fiber structure," *Chinese Optics Letters*, 2018, 16(4): 040602.